Ground-Motion Simulations for the M 6.9 Irpinia 1980 Earthquake (Southern Italy) and Scenario Events

Gabriele Ameri[1], Antonio Emolo[2], Francesca Pacor[1] and Frantisek Gallovic[2,3]

[1]Istituto Nazionale di Geofisica e Vulcanologia, via Bassini 15, 20133, Milano, Italy

[2]Dipartimento di Scienze Fisiche, Università degli Studi "Federico II", Napoli, Italy

[3]Charles University, Faculty of Mathematics and Physics, Dept. of Geophysics, V Holesovickach 2, Praha 8, 180 00, Czech Republic

Address for correspondence:

Gabriele Ameri
Istituto Nazionale di Geofisica e Vulcanologia
Sezione di Milano-Pavia
Via Bassini, 15
20133 – Milano – Italy
E-mail: ameri@mi.ingv.it
Tel: +39 02 23699259

VERSION: 20 January 2010 (Accepted)

Submitted To: BSSA

Electronic Supplement includes 6 figures comparing observed and simulated acceleration and velocity seismograms and acceleration response spectra for the three considered simulation techniques.

Abstract

In this paper, we adopt three ground-motion simulation techniques (EXSIM, Motazedian and Atkinson, 2005, DSM, Pacor et al., 2005 and HIC, Gallovič and Brokešová, 2007), with the aim of investigating the different performances in near-fault strong-motion modeling and prediction from past and future events. The test case is the 1980, M 6.9, Irpinia earthquake, the strongest event recorded in Italy. First, we simulate the recorded strong-motion data and validate the model parameters by computing spectral acceleration and peak amplitudes residual distributions. The validated model is then used to investigate the influence of site effects and to compute synthetic ground motions around the fault. Afterward, we simulate the expected ground motions from scenario events on the Irpinia fault, varying the hypocenters, the rupture velocities and the slip distributions. We compare the median ground motions and related standard deviations from all scenario events with empirical ground motion prediction equations (GMPEs). The synthetic median values are included in the median ± one standard deviation of the considered GMPEs. Synthetic peak ground accelerations show median values smaller and with a faster decay with distance than the empirical ones. The synthetics total standard deviation is of the same order or smaller than the empirical one and it shows considerable differences from one simulation technique to another. We decomposed the total standard deviation into its between-scenario and within-scenario components. The larger contribution to the total sigma comes from the latter while the former is found to be smaller and in good agreement with empirical inter-event variability.

1. Introduction

One of the key steps of a seismic hazard assessment study is the prediction of ground-motion parameters, assuming the occurrence of specific earthquakes. This goal may be easily pursued using Ground-Motion Prediction Equations (GMPEs) that provide the probability distribution of earthquake ground motion at a given site as a function of e.g., magnitude, distance, site condition and fault mechanism (Ambraseys et al., 2005; Boore and Atkinson 2008; Bindi et al., 2009; Akkar and Bommer, 2010; among many others). Although they are retrieved through the analysis of recorded strong-motion data, the GMPEs account only for the average characteristics of the earthquake source and wave propagation processes. In general, at distances comparable with the fault dimensions, the complexity and heterogeneity of the source rupture process may strongly influence the ground motion, especially in the case of moderate-to-large earthquakes (Archuleta and Hartzell, 1981; Heaton, 1990). This feature is crudely accounted for by GMPEs, due to the simplistic source parameterization adopted in the functional forms, and to the paucity of strong-motion data recorded at near-source distances for large magnitudes. This is the case of Italy, where only few strong-motion data recorded in the proximity of the rupturing fault are available, even in the case of moderate-to-large instrumental earthquakes (Luzi et al., 2008; http://itaca.mi.ingv.it/ItacaNet/).

An alternative approach to predict earthquake ground motions is represented by the simulation of synthetic accelerograms through either purely stochastic or hybrid deterministic-stochastic methods. These methods are able to generate realistic seismograms, in the frequency band of engineering concern, close to the causative fault (e.g., Zollo et al. 1997; Mai and Beroza, 2003; Motazedian and Atkinson, 2005; Pacor et al., 2005; Gallovič and Brokešová, 2007;) and can be used to perform earthquake scenarios studies (Aagaard et al., 2008; Ameri et al., 2008; Cultrera et al., 2010). However, these methods are generally considered as advanced tools in hazard

assessment framework, since, compared to GMPEs, they require a larger number of seismological information about the earthquake source and the propagation medium, which are often uncertain.

The most widely used simulation techniques are based on a kinematic model of the extended source and require the specification of parameters describing the rupture evolution (slip function, rupture velocity, nucleation point position, etc.). These parameters have to be sought when one is interested in reproducing strong-motion records associated with an occurred earthquake (Mena et al., 2006; Ameri et al., 2009). On the contrary, when seismic hazard studies and earthquake scenarios are carried out, it is needed to vary the parameters describing the rupture evolution, in order to producing a large number of scenario events. This approach is supported by the fact that it is not possible to predict which rupture scenario will occur on a seismogenic fault. In this way, various possible rupture processes, occurring on the same fault, are simulated and, for each of them, synthetic seismograms are computed. The required strong-motion parameters at the site of interest are then expressed through a statistical analysis of the simulated seismograms (Convertito et al., 2006; Emolo et al., 2008; Cultrera et al., 2010; Chiauzzi et al., 2010) and the associated variability may be studied and quantified (Ripperger et al., 2008).

The approximations introduced in the numerical representation of the rupture and wave propagation processes entail, however, that the ground-motion simulated at a given site by different techniques is generally different in some features (e.g., signal duration, peak values in specific frequency ranges, etc.). As a consequence, some techniques could not be able to reproduce specific ground-motion characteristics as e.g., directivity pulses or polarization of ground motion.

Furthermore, synthetic seismograms should be validated in some way, in order to demonstrate the reliability of the ground motions estimates. Some examples can be found in Convertito et al.

(2006), Sørensen et al. (2007), Gallovič and Burjánek (2007), Gallovič and Brokešová (2007), Ansal et al. (2008), Ameri at al. (2008), Emolo et al. (2008), Cultrera et al., (2009), Graves and Pitarka, (2010).

In this paper, we apply three finite-fault simulation techniques to reproduce the ground motion during the 1980, M 6.9, Irpinia (southern Italy) earthquake and generate scenario events. The aim is to investigate the different performances of the simulation techniques in near-fault strong-motion modeling and prediction from past and future events. First, we synthesize accelerometric records at some of the near-fault sites that recorded the Irpinia earthquake and evaluate the capability of the simulation methods to reproduce the main features (amplitude and frequency content) of observed strong-motion data. Then, we compute synthetic accelerograms at a dense grid of virtual observers, simulating a large number of possible scenario events. We produce, for each simulation technique, synthetic datasets that we treat statistically in order to evaluate the median ground motion and the associated variability. In particular, similarly to what is done in the framework of the GMPEs (e.g., Atik et al.; 2010), we separate the total variability in the inter-scenario (between scenario) and intra-scenario (within scenario) components. The inter-scenario component measures the variability among the average ground motions predicted by all scenario events, and the intra-scenario variability measures the variability of the ground motion with respect to the average motion predicted for each earthquake scenario.

2. Simulation methods

In this work, we use three well-known simulation methods: the stochastic EXSIM code (Motazedian and Atkinson, 2005; Boore, 2009), the hybrid deterministic-stochastic approach with approximated Green's functions (DSM, Pacor et al., 2005) and the broadband integral-composite technique with full-wavefield Green's functions (HIC, Gallovič and Brokešová, 2007). Table 1 summarizes the main characteristics of each technique in terms of source and path

parameterization and Table 2 reports the input modeling parameters later described. Here, we recall some key elements about the source representation for each technique and refer, for further explanation, to the abovementioned reference papers.

The EXSIM and DSM techniques are both an extension of the point-source stochastic method (Boore, 1983; 2003) to include the rupture propagation along an extended fault. The kinematic rupture model is simply described assigning the slip distribution, the rupture velocity and the nucleation point on the fault. In EXSIM, the fault is divided into N sub-faults and each of them is considered as a point source, emitting an ω-square spectrum. Ground motions produced by sub-faults are summed in the time domain, with a proper time delay, to obtain the ground motion from the entire fault. The DSM generates acceleration envelopes using the isochrone theory (Bernard and Madariaga, 1984; Spudich and Frazer, 1984). For a given site, each instant of time of the envelope is constructed by summing the contributions to ground motion from the corresponding isochrone on the fault. The spectral content of the synthetic seismogram is then defined through a reference spectrum. This spectrum corresponds to an ω-square model, with fixed corner frequency (hereinafter referred as DSM_{fix}) or with apparent corner frequency (hereinafter referred as DSM_{app}), given by the inverse of the envelope duration, different from site to site. In this latter case the directivity-induced amplification effect on the ground motion related to the rupture propagation along the extend fault, are included into the in the ω-square spectrum by the apparent corner-frequency.

The HIC technique simulates the rupture process in terms of slipping of elementary sub-sources with fractal number-size distribution (fractal dimension 2), randomly placed on the fault plane. At low frequencies, the source description is based on the representation theorem (integral approach, Aki and Richards, 2002) assuming a final slip distribution composed from the subsources, which is characterized by a k-squared decay (Herrero and Bernard, 1996; Gallovič and

Brokešová, 2004). At high frequency, instead, the ground-motion synthesis is obtained summing the contributions from each individual sub-source treated as a point-source (composite approach). The Green's functions for both frequency bands are evaluated by the discrete wave-number technique (Bouchon, 1981) in a layered 1D medium.

3. The November 23, 1980, M 6.9, Irpinia earthquake

The November 23, 1980, M 6.9, Irpinia earthquake (southern Italy) is the strongest earthquake instrumentally recorded in Italy. The earthquake was widely studied and a complete review was published on a Special issue of Annals of Geophysics (Vol. XXXVI, n.1, 1993). It was a normal-faulting complex event that involved at least three distinct shocks starting in a time span of approximately 40 seconds (Figure 1): the main event (further referred to as 0s event) was followed by two further rupture episodes delayed about 20s and 40s, respectively (Bernard and Zollo, 1989; Pantosti and Valensise, 1990). The characteristics of the 0s event have been deeply investigated (Cocco and Pacor, 1993; Giardini, 1993; Pingue et al., 1993) and this shock was related to the rupture of a normal fault striking in the Apennine direction and dipping 60° toward southeast (Table 2).

The earthquake triggered 21 analog accelerometric stations, 10 of them at epicentral distances within 60 km (Working Group ITACA, 2009, and Figure 1). The near-fault strong motion records are characterized by a very long duration, about 80s, and the three events can be clearly detected with the exception of the southernmost stations, BRN and ALT, that were likely triggered by the 20s event. The recording stations in epicentral area are classified mostly as rock and stiff sites. All information related to their geological and geotechnical characteristics are taken from the corresponding monographs recently published in the Italian strong-motion database (Working Group ITACA, 2009).

We selected 7 near-fault stations that clearly recorded the 0s event and are weakly affected by site effects (Table 3). The maximum peak acceleration (PGA) and velocity (PGV) values (3.01 m/s^2 and 0.70 m/s, respectively) were recorded at STR on the EW component. These high peak ground motions may be ascribed to directivity effects related to the position of the site with respect to direction of the rupture propagation on the 0s fault (Cultrera et al., 2010).

A rough estimation of the frequency content of the records may be inferred by the PGA/PGV ratio (Kwon and Elnashai, 2006), that is equal to 0.58±0.11 g/ms^{-1} considering the mean ratio for data in Table 3. Following the classification by Zhu et al. (1988) and Kwon and Elnashai (2006), the 1980 Irpinia near-fault ground motions can be classified as High Velocity-Low Acceleration (HV-LA) records. Low PGA/PGV ratios signify earthquakes with low predominant frequencies, broader response spectra and longer duration (Kwon and Elnashai, 2006). Other earthquakes in different tectonic environments (e.g., the M_w7.4, 1999 Chi-Chi earthquake) show similar HV-LA behavior.

3.1 Source and propagation models

In this work we used the fault geometry and 1D crustal model (Table 2 and Table 4) as described by Cultrera et al. (2010), that simulated seismic scenarios from different rupture models of the 0s fault, in order to study the source-related variability of low-frequency ground motions. The kinematic rupture model considered for the 0s fault is based on the study of Cocco and Pacor (1993): the final slip distribution is characterized by two main asperities, the largest located close to southern edge of the fault and the other to northern edge, both at a depth between 6.5 and 11 km. Starting from the slip and rupture time distributions originally proposed by the authors, we calculated a k^{-2} slip model (Herrero and Bernard, 1994; Gallovič and Brokešová, 2004) shown in the top panel of Figure 2. The position of the nucleation point (largest star in the top panel of Figure 2) corresponds to the instrumental epicenter (40.76°N, 15.31°E; Working group ITACA, 2009) and the rupture velocity was set at 0.8Vs, where Vs is the shear-wave velocity (see Table 4).

The spectral attenuation was defined in terms of quality factor *Q* and high-frequency decay parameter κ (Anderson and Hough, 1994). The depth-dependent Qp and Qs values used for HIC simulations are reported in Table 4. In DSM and EXSIM, a Q_S=100 was adopted in order to obtain results comparable with HIC simulations and as reported by Cultrera et al. (2010). We set κ = 0.03s, according to literature estimates for rock and stiff sites (Margaris and Boore, 1998; Bindi et al., 2004).

A crustal amplification function has been used in EXSIM and DSM simulation techniques to account for frequency-dependent amplification of seismic waves through the S-waves velocity profile of the crustal model (Boore and Joyner, 1997). For the Irpinia area, we adopted an amplification function for hard-rock sites (Siddiqqi and Atkinson, 2002; Atkinson and Boore, 2006), characterized by a shear-wave velocity near the surface of about 2000 m/s (class A according to the NEHRP, 1994, classification) that is comparable with the velocity we used (Table 4).

The value of the stress parameter $\Delta\sigma$ has been set to 80 bar on the basis of a trial-and-error analysis performed through the comparison of observed and synthetic high-frequency level of the Fourier amplitude spectra (S3 project deliverable D0, 2007).

The input parameters for the three techniques adopted to simulate the 0s events are summarized in Table 2.

3.2 Modeling of the Strong-Motion Data

We calculated the synthetic seismograms at the selected stations using the three simulation techniques and adopting the source and propagation models described above (Table 2 and Table 4). The comparisons with the recorded data, in terms of acceleration and velocity waveforms (NS and EW components) and acceleration response spectra (SA, 5% damping), in the frequency band 0.1–12 Hz, are reported in Figures S1 to S6 of the electronic supplements. Here, as example, we show the results for HIC technique (Figure 3). The HIC synthetics are the most suitable to discuss

the goodness of the adopted rupture and propagation models, since this approach adopts complete Green's functions and solves deterministically the representation theorem at low frequencies.

For most of the sites, the simulated time series are in good agreement with the recorded ones, both in time and frequency domains. The good fit for BGI station, located just a few kilometers from the fault support the reliability of the adopted rupture model. Also the waveforms at the furthest stations, BVN and BNV, located at about 30 km from the fault, are well simulated, indicating that the 1D propagation model accounts for the main observed phases. BSC synthetics spectra well reproduce the observed ones at frequency larger than 1 Hz. The misfit at lower frequencies (around 0.5 Hz), is likely due to the velocity inversion in the soil profile below the station (Olivares and Silvestri, 2001; Cultrera et al., 2010), not accounted for in the simulations.

A worse fit is obtained for CLT, RNR and STR, where the observed ground motion is underestimated. Indeed, at CLT, the HIC synthetics are not able to simulate the large amplitude of the later arrivals while, at RNR, the waveforms are deficient of high-frequency energy. Finally at STR, distant less than 5 km from fault, we are only able to fit the first large phases of the NS component. The lower ground motion amplitude simulated in the EW direction can be ascribed to the effect of the radiation pattern. This is not observed in the records, likely due to the small-scale variations of the source mechanism, not included in the model.

Regarding the other two simulation techniques (Figures S2, S3, S5 and S6), the use of simplified Green's functions does not allow to reproduce correctly the phases of the observed seismograms. The spectral content and peak amplitudes are well reproduced at BGI and BSC and, similarly to HIC, RNR, CLT and STR are underestimated.

To summarize the modeling results and to assess the performance of the simulation techniques, we computed the SA, PGA and PGV residuals ($\log_{10}$[observed/simulated]) at each

stations. SA residuals at each frequency are then averaged over the 7 stations, yielding a measure of the model bias (Figure 4). In general, the simulations provide small model biases, with a tendency to positive values, (i.e., average underestimation) over the entire frequency range. This result is expected since the synthetics are simulated at bedrock, while the recording sites, although located on stiff soils, are characterized by variable local geology. Nevertheless, the models biases do not exceed 0.25 which means an average underestimation of less than a factor of 2. HIC residuals are less scattered at low frequencies (< 1Hz) while EXSIM and DSM have a similar σ_{bias} (i.e., similar scatter of the residuals), with a tendency to lower sigma in the mid-frequency range ($\sigma_{bias}\approx0.15$). and higher values at both low and high frequencies ($\sigma_{bias}\approx0.25$). The positive and negative residuals outside the standard deviation are related to RNR, CLT and STR sites, as already noted in Figure 3.

Possible site amplification at these stations are evaluated computing the Horizontal-to-Vertical Spectral Ratios (HVSR) (Lermo and Chavez-Garcia, 1993), using all the strong-motion data available (Figure 5). RNR, located on volcanic rocks, shows flat HVSR, while small broadband amplifications are obtained at CLT and STR, installed on silty clays and weathered sandstone, respectively. Note that the paucity of strong motion data at RNR (3 records) together with possible amplification on the vertical component may lead to not reliable HVSR results.

The STR and CLT HVSR mean amplification curves are used to multiply the Fourier amplitude spectra of the synthetics computed at bedrock, maintaining the phases unchanged. The geometric mean acceleration response spectra of amplified synthetic time series are shown in Figure 6. In general, the fit improves, with the exception of HIC results at CLT. In this case an overestimation of the high-frequency content (f > 2Hz) is observed and further investigations may be carried out to explain the role of the site response at this station.

In conclusion, due to the relatively small number of records considered, it is difficult to establish which method performs better in the modeling of the 1980 earthquake strong-motion data. We note a general consistency among the simulation results in terms of spectral accelerations and peak values whereas the synthetic waveforms show notable differences in duration and phase. Moreover, the effect of local site amplification seems not remarkable at the considered stations, except at RNR, where we are not able to explain the high-frequency content of the observed waveforms with the adopted source, propagation and site parameters. Overall, the results presented in Figure 3 and 4 make us confident that the methods can be used to predict the bedrock ground motion associated to the 1980 and other scenario events for the study area.

3.4 Ground-motion scenario

The validated model is used to simulate the ground motion for the 0s event at a dense grid of 86 virtual receivers (their position is shown in Figure 1), in order to evaluate the spatial distribution of the ground motion predicted by the three methods. The PGA and PGV maps computed for bedrock sites are shown in the Figure 7. For all the simulation techniques, the finite dimension of the fault produces contour lines slightly elongated in the fault-strike direction. Moreover, the ground motion decays more slowly in the north-western direction, i.e., in the direction toward which the rupture propagates, than in the opposite direction.

The PGA maps simulated with DSM_{fix}, EXSIM and HIC techniques show an almost isotropic distribution with respect to the fault projection, since similar approaches are implemented in modeling the high-frequency component of the radiation emitted by the extend source. For instance, in HIC technique, the high-frequency content is simulated through an incoherent sum of the energy emitted by stochastic elementary sub-sources (composite approach), resulting rather independent from the source-to-receiver azimuth (see also Gallovič and Burjanek, 2007). On the other hand, the rupture directivity effects on the ground motion are evident in the HIC PGV map,

where the area of maximum is shifted far from the epicenter and close to the BGI and STR stations. This is caused by the deterministic calculation of ground motion at low frequencies (mostly affecting the PGV), preserving the inherent directivity effect. In particular, the large PGV area in Figure 7a is due to the combined effect of the north-western and up-dip rupture propagation, position of the second asperity (top panel of Figure 2), and radiation pattern.

We also showed in Figure 7d the maps, generated with DSM_{app}, in order to evaluate the influence of the apparent-corner-frequency approach on the spatial distribution of ground motion. The peak ground motions strongly change with respect to DSM_{fix}, predicting large amplitudes close to the northwestern edge of fault, thus modeling the effect of rupture directivity on both simulated PGA and PGV. The difference between the DSM_{fix} and DSM_{app} predictions is due to the use of different corner frequencies in the source spectrum. In the first case, following the classical ω-square model, the corner frequency is defined as $f_c=4.9 \times 10^6 V_s(\Delta\sigma/M_0)^{1/3}$,assuming a fixed value for all sites. In the second case, the corner frequency is calculated as the inverse of the source duration as perceived at each site (i.e., apparent corner frequency). For example, in section 3.2, a corner frequency f_c=0.11 Hz is obtained adopting $\Delta\sigma$=80 bar. On the other hand, the apparent corner frequency obtained at STR and CLT sites is f_a=0.16 Hz and f_a=0.05 Hz, respectively. Since the high-frequency plateau of the acceleration source spectrum in the ω-square model is proportional to $M_0 f_c^2$ it is clear that the two approaches can lead to very different simulated ground motions.

Although based on different approaches, DSM_{app} and HIC generate consistent PGV distributions. On the other hand, DSM_{app} generate high PGA values close to STR station and small values at sites located in the opposite direction (e.g., RNR, CLT). Such large differences are, however, not observed in the records, suggesting that DSM_{app} might overemphasize the forward and backward directivity effects close to the fault.

To verify the reliability of the ground motion scenario for the 0s event, computed from the three simulation techniques, the synthetic PGA and PGV values are compared with predictions from Akkar and Bommer (2010), AkB10, GMPEs (Figure 7, right panels) .

For the three simulation techniques, the synthetic PGAs underestimate the empirical median prediction and show a stronger attenuation with distance, while the PGVs well match the median values, over the considered distance range. Overall, the recorded peaks are better fitted by the synthetics both for acceleration and velocity.

The HIC PGV and DSM_{app} PGA and PGV values as a function of distance are largely scattered and some values are outside of the AkB10 standard deviation. This scatter is caused by the concurrent presence, at similar R_{JB} distances, of receivers that experience both forward and backward directivity.

The ground-motion scenarios for the 0s event show PGA that are, on average, smaller and decay faster with distance than the average predictions from the considered GMPE, confirming the HV-LA property observed from the Irpinia earthquake records. The average simulated PGA/PGV ratios are 0.71±0.50 g/ms^{-1} for HIC, 0.49±0.12 g/ms^{-1} for EXSIM, 0.60±0.16 g/ms^{-1} for DSM_{fix} and 0.57±0.15 g/ms^{-1} for DSM_{app}.

4. Ground motion prediction for M_w 6.9 scenario events.

The next step of this study is the generation of ground motion scenarios at bedrock, associated with a fault having the geometry, orientation, and seismic moment of the 0s fault in order to characterize the potential variability in ground motions for future events of this size on the Irpinia fault. The variability related to local site response is not included in this analysis.

A similar study was performed by Cultrera et al. (2010) using a discrete-wavenumber/finite-element technique with the aim of investigating the low-frequency parametric variability of the ground motion (up to 2 Hz) as a function of different source parameters (i.e., rupture velocity, slip

distribution, nucleation point, and source time function). They showed how the distributions of spectral displacement at 2 seconds and of PGV depend on both azimuth and distance and how the simulated ground motion is influenced by the source parameters. In this study we extend the scenario-events analysis to intermediate and high-frequency range and summarize the results estimating the median ground motion values and the standard deviations associated with the parametric uncertainties of the model.

We constructed a large set of possible rupture models for various positions of the rupture nucleation point, final slip distributions on the fault and rupture velocity values. The first set of scenario rupture models uses the same distribution of slip (Figure 2, top panel) and rupture velocity (0.8Vs) as for the simulation of the 1980 earthquake records; however we considered 6 additional hypocenter locations spanning the length of the fault at a depth of about 11 km (Table 2). Further sets of rupture models were generated considering two alternative slip distributions with the same average slip value and different position of asperities (Figure 2) and two alternative values of rupture velocities (0.7Vs and 0.85Vs). The two additional slip models are characterized by asperities located on the central portion and on the northwestern portion of the fault, respectively. Note that the same suite of hypocenters and rupture velocities is used for each slip distribution.

For each kinematic rupture model we simulated the time series considering the same receivers grid of Figure 1 and using HIC, EXSIM and DSM_{app} techniques. Note that we did not include DSM_{fix} method as we have shown that it practically provides identical results to EXSIM. In total, for each technique, a data set composed of about 4500 accelerograms was produced, obtained by the combination of 54 rupture models and 84 virtual observers radially distributed within 50 km to the fault. The distribution of simulated PGA and PGV from all the considered rupture models, as a function of R_{JB}, is presented in Figure 8.

We compared simulated peak ground motions in terms of median estimates and related variability. We calibrated a simple functional form for the three synthetic data sets, using a similar approach as in empirical GMPEs. Here, no dependence on magnitude, anelastic attenuation term, and focal mechanism are introduced as magnitude and focal mechanism is fixed parameters in the simulations (M_w6.9, normal fault) and the distance range is within 50 km.

A regression scheme based on the random effect model (Brillinger and Preisler 1985; Abrahamson and Youngs 1992) was adopted in order to decompose the total variability into its components (Strasser et al., 2009; Atik et al., 2010). To keep the terminology clear, we will refer to inter-scenario (i.e. between-scenario) and intra-scenario (i.e. within-scenario) variability (instead of inter-event and intra-event variability) as we are not dealing with different events, strictly speaking.

The regressions were performed for the geometric mean of the NS and EW components of peak ground motions. The assumed functional form is given by

$$\log_{10} Y = a + c \log_{10} \sqrt{\left(R_{JB}^{\ 2} + h^2\right)} + \delta_{K,i} + \delta_{A,ij} \qquad (1)$$

where Y is the response variable (i.e., PGA or PGV); h = 10.9 km (the depth of the hypocenter in the source model), a and c are the coefficients of the regression and $\delta_{K,i}$ and $\delta_{A,ij}$ represent the inter-scenario (depending on scenario-event i only) and intra-scenario (depending both on scenario-event i and site j) residuals, assumed to be normally distributed with variances σ^2_K and σ^2_A, respectively. σ^2_K and σ^2_A represent, the variability of median ground motions predicted for the various scenario events, and the variability of ground motion with respect to the median motion predicted for each individual scenario event.

The total variance of model (1) is given by

$$\sigma^2_{TOT} = \sigma^2_K + \sigma^2_A \qquad (2)$$

Table 5 lists the regression coefficients and sigma values. Figure 8 shows the median curves ± σ_{TOT} estimated from equations (1) and (2), considering PGA and PGV calculated for the three data sets. The median ground motion values of the three simulation methods are consistent, while the relative standard deviations show significant differences, also depending on the considered strong-motion parameter (see Table 5).

The observed difference in the total sigma values implies that DSM_{app} synthetics present the largest PGA variability whereas only half of such variability is found for EXSIM and HIC peak accelerations. On the other hand, comparable PGV variabilities are found for HIC and DSM_{app}, while smaller variability is observed from the EXSIM simulations. The inter-scenario (σ_K) and intra-scenario (σ_A) variabilities reveal that the larger contribution to the total sigma comes from the latter (i.e., spatial) variability. Moreover, it can be noticed that the inter-scenario standard deviations present the lowest values for EXSIM synthetics whereas DSM_{app} and HIC peaks are characterized by similar σ_K, though HIC inter-scenario variability substantially increases for PGVs. These differences in σ_K values signify that the influence of the parametric uncertainties on ground-motion estimates is different for each technique EXSIM method results loosely sensitive to variations in slip distribution and rupture velocity of the kinematic model. Conversely, in DSM_{app}, the calculation of isochrones and of the use of the apparent corner frequency, implies that the choice of the nucleation point position and of the value of rupture velocity has a large influence on the simulated ground motion. Finally, HIC synthetics, characterized by the largest inter-scenario variability, are calculated solving the representation theorem at low frequency. As PGV is sensitive to the intermediate frequency of the motion (where the deterministic and stochastic approaches are merged) we expect to observe a larger dependence on the source parameters (e.g., hypocenter location and slip distribution) than for stochastic methods.

4.1 Comparison with GMPEs

In Figure 9 (top panels) the median PGA and PGV curves from simulated data sets are compared with the median ± 1σ of the AkB10 empirical GMPEs (AkB10 for M_w=6.9) for rock site class.

The synthetic PGA and PGV median curves are enclosed in the empirical standard deviation, but simulated PGAs exhibit a different decay with distance, attenuating faster for R_{JB} larger than 10 km. This feature, already observed in Figure 7, is common to the all examined rupture scenarios and can not be considered a peculiarity of the 1980 Irpinia earthquake.

Regarding the synthetics variability (Table 5), the DSM and HIC total standard deviations for PGV are consistent with the AkB10 standard deviation. Conversely, the total synthetic sigma for PGA is similar only for DSM_{app}, while it is significantly smaller for the other two simulation techniques.

The median PGA and PGV ± inter-scenario (σ_k) and intra-scenario (σ_A) for HIC are compared with AkB10 predictions, considering the inter-event and intra-event standard deviations, separately (Figure 9, middle and bottom panels). Synthetic inter-scenario and empirical inter-event standard deviations have very similar values both for PGA and PGV, suggesting that the observed ground motion variability associated to event-specific factors that we have not taken into account (e.g., stress drop, focal depth, etc.) is of the same order of magnitude of the variability caused by different rupture scenarios on the given fault.

In Figure 9 (bottom panel), we observe that the synthetic intra-scenario standard deviation is similar to the empirical one for PGV (right panel) and lower for PGA (left panel). This result means that, at low-to-intermediate frequencies (affecting the PGV), the observed ground motion spatial variability, including effects depending on record-specific factors (e.g., directivity effects, different response for rock sites, etc.) is of the same order of magnitude of the synthetics one. The synthetic intra-scenario variability account for directivity effects, radiation pattern, source-sites geometry, but the site condition is equal for all sites. Thus, the larger values of PGA empirical intra-event

standard deviation as compared with synthetic one may be explained both by the lack of directivity effects at high-frequencies in the synthetics and/or by the randomness in site response for rock sites that can make an important contribution in the observed high-frequency ground motion variability.

Finally, we observe (Table 5) that DSM_{app} provides a PGA intra-scenario variability larger than the AkB10 one. This can be ascribed to the overestimation of the spatial variability related to directivity effects as shown in Figure 7.

5. Conclusions

In this paper we performed a simulation study for the 1980, M 6.9, Irpinia (Southern Italy) earthquake. This seismic event is the largest instrumental earthquake recorded in Italy and it involved three distinct shocks. We focused our attention on the 0s event, which ruptured the largest fault segment.

The modeling of this event was performed with three finite-fault simulation methods, i.e., the finite-fault stochastic method (EXSIM, Motazedian and Atkinson, 2005; Boore, 2009), the hybrid deterministic-stochastic method (DSM, Pacor et al., 2005) and the broadband integral-composite approach (HIC, Gallovič and Brokešová, 2007), assuming the geometry and source kinematic models based on Bernard and Zollo (1989) and Cocco and Pacor (1993). To validate the model parameters, we first calculated synthetic seismograms at bedrock, in correspondence of 7 strong-motion stations, classified as rock or stiff sites. We found a general consistency among the simulation results in terms of spectral accelerations and peak values, whereas the synthetic waveforms show remarkable differences in duration and phase. The goodness of fit of the modeling was then assessed by evaluating a model bias, based on acceleration response spectra residuals, that resulted within a value of ±0.25 (in $\log_{10}$ units) around zero for all the techniques. We verified that the local site response do not have predominant effect on ground motion at the

investigated stations, expect at RNR, where we were not able to explain the high-frequency content of the observed waveforms with the adopted source, propagation and site parameters.

The validated model was used to simulate the ground motion from the 0s event at a regular grid of virtual receivers in order to study the ground motion features at regional scale. Due to the particular position of hypocenter, we found peak distributions elongated approximately in the fault-strike direction. HIC and DSM_{app} techniques predicted larger PGV values toward the north-west as effect of rupture directivity both along the strike and up-dip directions.

The second part of this study concerned the simulation of ground motions from scenario events associated with the 0s seismogenic fault. We considered 54 different rupture models combining three slip distributions, three rupture velocities, and six positions of the hypocenter. We calculated the synthetic accelerograms, produced by each of the rupture processes, at a grid of 84 virtual receivers radially distributed within 50 km around the fault, with three simulation techniques. In this way, we construct a data set of more than 4500 synthetic seismograms for each technique, suitable for statistical analyses. We used each synthetic data set to calibrate a simple functional form in order to describe the attenuation with distance of simulated motions from many rupture scenarios in terms of median PGA and PGV and related variability. From the regression analysis we found that the median curves of simulated ground motions are consistent even if the simulation techniques describe in different ways the source and the wave propagation processes. On the other hand, the total variability differs from one technique to another. This means that the effect of the parametric uncertainties of simulated ground motions depend on the simulation method.

We compared the synthetic predictions with the empirical GMPEs and we found that the PGA synthetic median curves are smaller and exhibit a faster decay with distance than the GMPEs. Since the attenuation model used in the simulations have been validated with the data recorded

during the 1980 Irpinia earthquake, we conclude that the considered empirical GMPEs for PGA may be too conservative in case of occurrence of the assumed scenario events.

We also compare the empirical and synthetic standard deviations. Note that, formally, the two quantities describe different components of the total variability in ground motion prediction: the modeling variability (for empirical GMPEs) and the parametric variability (for simulations) (see Toro et al., 1997). When comparing ground motions variability from GMPEs and synthetics from scenario events we have to consider that, on one hand, the constructed scenarios account for the uncertainties of a few source parameters, while other sources of variability (e.g., differences in focal mechanism, site conditions, etc.) considered in GMPEs are fixed in the simulations. On the other hand, the synthetic motions are computed on a much denser distribution of sites around the fault with respect to what observed in real earthquakes accounting for a more complete characterization of the spatial distribution of near-fault ground motions. Moreover the simulations evaluate the ground-motion variability from different ruptures on the same fault, while, due to the actual lack of such episodes, this variability is missing in GMPEs (Cultrera et al., 2010).

The inter-scenario (σ_K) and intra-scenario (σ_A) variabilities reveal that the larger contribution to the total sigma comes from the latter (i.e., spatial variability). The EXSIM synthetics are characterized by the smallest inter-scenario variability while the HIC ones by the largest (especially for PGV) due to the deterministic calculations of the motion at low frequencies. The DSM_{app} synthetics present the largest intra-scenario variability which means that, on average, the simulations produce the largest spatial variability of ground motion. This is consistent with the large sensitivity of DSM_{app} method to the position of the nucleation point that directly affects the rupture directivity (Ameri et al., 2009) producing large spatial variation of ground motion around the fault. Although high-frequency directivity effects have been observed on strong-motion records from recent moderate-magnitude earthquakes (i.e. 1997, M 5.6-6.0,Umbria-Marche

events (Castro et al., 2001; Castro et al., 2008; Emolo et al., 2008); 2009, M 6.3, L'Aquila earthquake (Akinci et al.; 2010) further studies should be carried out to understand if this phenomena could significantly affect the observed ground motion variability even in this frequency range.

Data and Resources

Seismograms recorded during the 1980 Irpinia earthquake used in this study can be downloaded from the Italian Accelerometric Archive (ITACA) at http://itaca.mi.ingv.it (last accessed January 2011).

The EXSIM code has been downloaded from http://www.daveboore.com/software_online.htm (last accessed January 2011)

Some plots were made using the Generic Mapping Tools version 3.3.6 (Wessel and Smith, 1998; http://www.soest.hawaii.edu/gmt/ last accessed January 2008).

Acknowledgements

This research was funded by DPC - INGV agreement 2004–2007 within the project titled "S3– Shaking and damage scenarios in area of strategic and/or priority interest" and supported by Grant Agency of the Czech Republic (205/08/P013). We thank the associate editor Hiroshi Kawase, Giovanna Cultrera and an anonymous reviewer for constructive comments and criticism that greatly improved the quality of the original manuscript. We thank Gail Atkinson, Dariush Motazedian and David Boore for providing the EXSIM code.

References

Aagaard B. T., T. M. Brocher, D. Dolenc, D. Dreger, R.W. Graves, S. Harmsen, S. Hartzell, S. Larsen, K. McCandless, S. Nilsson, N. A. Petersson, A. Rodgers, B. Sjögreen, and M. L. Zoback (2008). Ground Motion Modeling of the 1906 San Francisco Earthquake, Part II: Ground-Motion Estimates for the 1906 Earthquake and Scenario Events. Bull. Seism. Soc. Am. 98, 1012–1046

Abrahamson N. A. and R. R. Youngs (1992). A stable algorithm for regression analyses using the random effects model. Bull. Seism. Soc. Am. 82, 505–510.

Aki K. and P.G. Richards (2002). Quantitative seismology, 2nd edition. University Science Books, 704 pp.

Akinci, A., Malagnini, L. and F. Sabetta (2010). Characteristics of the strong ground motions from the 6 April 2009 L'Aquila earthquake, Italy. Soil Dyn. Earthquake Eng, 30, 320-335.

Akkar S. and J.J. Bommer (2010). Empirical Equations for the Prediction of PGA, PGV and Spectral Accelerations in Europe, the Mediterranean Region, and the Middle East. Seism. Res. Lett. 81, 195-206.

Amato A. and G. Selvaggi (1993). Aftershock location and P-velocity structure in the epicentral region of the 1980 Irpinia earthquake. Ann. Geophys. 36, 3-15.

Ambraseys N. N., J. Douglas , S.K. Sarma and P.M. Smit (2005). Equations for the estimation of strong ground motions from shallow crustal earthquakes using data from Europe and Middle East: horizontal peak ground acceleration and spectral acceleration. Bull. Earthq. Eng. 3, 1–53.

Ameri G., F. Pacor, G. Cultrera and G. Franceschina (2008). Deterministic ground-motion scenarios for engineering applications: the case of Thessaloniki, Greece. Bull. Seism. Soc. Am. 98, 1289–1303.

Ameri G., F. Gallovič, F. Pacor and A. Emolo (2009). Uncertainties in strong ground-motion prediction with finite-fault synthetic seismograms: an application to the 1984 M 5.7 Gubbio, central Italy, earthquake. Bull. Seism. Soc. Am. 99, 647–663.

Anderson J.G. and S.E. Hough (1984). A model for the shape of the Fourier amplitude spectrum of acceleration at high frequencies. Bull. Seism. Soc. Am., 74, pp. 1969–1993.

Ansal A., A. Akinci, G. Cultrera, M. Erdik, V. Pessina, G. Tonuk and G. Ameri (2008). Loss estimation in Istanbul based on deterministic earthquake scenarios of the Marmara Sea region (Turkey). Soil Dyn. Earth. Eng. 29, 699–709.

Archuleta R. J. and S. H. Hartzell (1981). Effects of fault finiteness on near-source ground motion. Bull. Seism. Soc. Am. 71, 939-957.

L. A. Atik, N. Abrahamson, J. J. Bommer, F. Scherbaum, F. Cotton, and N. Kuehn (2010). The Variability of Ground-Motion Prediction Models and Its Components. Seism. Res. Lett., 81(5), 794 - 801

Atkinson G. M. and D. M. Boore (2006). Earthquake ground-motion prediction equations for eastern North America. Bull. Seism. Soc. Am. 96, 2181-2205.

Bernard P. and R. Madariaga (1984). A new asymptotic method for the modeling of near-field accelerograms. Bull. Seism. Soc. Am. 74, 539–558.

Bernard P. and A. Zollo (1989).The Irpinia (Italy) 1980 earthquake: detailed analysis of a complex normal faulting. J. Geophys. Res. 94, 1631-1647.

Bindi, D., Castro, R. R., Franceschina G., Luzi L., Pacor F. (2004). The 1997 - 1998 Umbria - Marche sequence (central Italy): Source, Path and Site effects estimated from strong motion data recorded in the epicentral area. J. Geophys. Res. 109, B04312, doi:10.1029/2003JB002857

Bindi D., L. Luzi, M. Massa and F. Pacor (2009). Horizontal and vertical ground motion prediction equations derived from the Italian Accelerometric Archive (ITACA). Bull. Earth. Eng. doi:10.1007/s10518-009-9130-9.

Boore D.M. (1983). Stochastic simulation of high-frequency ground motion based on seismological models of the radiated spectra. Bull. Seism. Soc. Am. 73, 1865–1894.

Boore D.M. (2003). Simulation of ground motion using the stochastic method. Pure Appl. Geophys. 160, 635–676.

Boore D.M. (2009). Comparing stochastic point-source and finite-source ground-motion simulations: SMSIM and EXSIM. Bull. Seism. Soc. Am. 99, 3202-3216.

Boore, D. M. and W. B. Joyner (1997). Site amplifications for generic rock sites, Bull. Seism. Soc. Am. 87, 327-341.

Boore D.M. and G.M. Atkinson (2008). Ground-motion prediction equations for the average horizontal component of PGA, PGV, and 5%-damped PSA at spectral periods between 0.01 s and 10.0 s. Earthq. Spectra 24, 99-138.

Bouchon M. (1981). A simple method to calculate Green's functions for elastic layered media. Bull. Seism. Soc. Am. 71, 959–971.

Brillinger D. R. and H. K. Preisler (1985). Further analysis of the Joyner–Boore attenuation data. Bull. Seism. Soc. Am. 75, 611–614.

Castro, R.R., A. Rovelli, M. Cocco, M. Di Bona, and F. Pacor (2001). Stochastic simulation of strong-motion records from the 26 September 1997 (Mw 6), Umbria-Marche (Central Italy) earthquake, Bull. Seism. Soc. Am., 91, 27-39.

Castro, R., R. F. Pacor, G. Franceschina, D. Bindi , C. Zonno and L. Luzi (2008). Stochastic Strong-Motion Simulation of the Mw 6 Umbria–Marche Earthquake of September 1997: Comparison of Different Approaches. Bull of Seism. Soc Am., 98, 2, 662–670, doi: 10.1785/0120070092.

CEN, Comité Européen de Normalisation (2004). Eurocode 8: Design of Structures for Earthquake Resistance—Part 1: General Rules, Seismic Actions and Rules for Buildings. Brussels: Comité Européen de Normalisation.

Chiauzzi L., A. Masi, M. Mucciarelli, M. Vona, F. Pacor, G. Cultrera, F. Gallovič and A. Emolo (2010). Building damage scenarios based on exploitation of Housner intensity derived from finite faults ground motion simulation. Submitted to Bulletin of Earthquake Engineering.

Cocco M. and F. Pacor. (1993). The rupture process of the 1980 Irpinia, Italy, earthquake from theinversion of strong motion waveforms. Tectonophys 218, 157-177.

Convertito V., A. Emolo and A. Zollo (2006). Seismic-hazard assessment for a characteristic earthquake scenario: an integrated probabilistic-deterministic method. Bull. Seism. Soc. Am. 96, 377-391.

Graves, R.W. and A. Pitarka (2010). Broadband Ground-Motion Simulation Using a Hybrid Approach. Bull. Seism. Soc. Am., 100, 2095 - 2123.

Cultrera G., F. Pacor, G. Franceschina, A. Emolo and M. Cocco (2009). Directivity effects for moderate-magnitude earthquakes (Mw 5.6–6.0) during the 1997 Umbria–Marche sequence, central Italy. Tectonophys. 476, 110-120.

Cultrera G., A. Cirella, E. Spagnuolo, A. Herrero, E. Tinti and F. Pacor (2010). Variability of kinematic source parameters and its implication on the choice of the design scenario. Bull. Seism. Soc. Am 100, 941 - 953.

Emolo A., G. Cultrera, G. Franceschina, F. Pacor, V. Convertito, M. Cocco and A. Zollo (2008). Ground motion scenarios for the 1997 Colfiorito, central Italy, earthquake. Ann. Geophys. 51, 509-525.

Gallovič F. and J. Brokešová (2004). The k^-2 rupture model parametric study: example of the 1999 Athens earthquake. Studia geoph. et geod. 48, 589-613.

Gallovič F. and J. Brokešová (2007). Hybrid k-squared source model for strong ground motion simulations: introduction. Phys. Earth Planet. Int. 160, 34–50.

Gallovič F. and J. Burjánek (2007). High-frequency directivity in strong ground motion modeling methods. Ann. Geophys. 50, 203-211.

Giardini D. (1993). Teleseismic observation of the November 23 1980, Irpinia earthquake. Ann. Geophys. 36, 17-25.

Heaton T. H. (1990). Evidence for and implications of self healing pulses of slip in earthquake rupture. Ph. Earth Planet. Int. 64, 1–20.

Herrero A. and P. Bernard (1994). A kinematic self-similar rupture process for earthquakes. Bull. Seism. Soc. Am. 84, 1216–1228.

Joyner W.B. and D.M. Boore (1981). Peak horizontal acceleration and velocity from strong-motion records including records from the 1979 imperial valley, California, earthquake. Bull. Seism. Soc. Am. 71, 2011–2038.

Kwon O. and A.S. Elnashai (2006). The effect of material and ground motion uncertainty on the seismic vulnerability curves of a RC structure. Engineering Structures 28, 289-303.

Improta L., M. Bonagura, P. Capuano and G. Iannaccone (2003). An integrated geophysical investigation of the upper crust in the epicentral area of the 1980, Ms=6.9, Irpinia earthquake (Southern Italy). *Tectonophysics*, 361,1-2, 139-169.

Lermo J and F.J. Chavez-Garcia (1993). Site effect evaluation using spectral ratio with only one station. Bull. Seism. Soc. Am. 83, 1574-1594.

Luzi L., S. Hailemikael, D. Bindi, F. Pacor, F. Mele and F. Sabetta (2008). ITACA (ITalian ACcelerometric Archive): a web portal for the dissemination of Italian strong-motion data. Seism. Res. Lett. 79, 716-722.

Margaris B.N. and D. M. Boore (1998) Determination of Aa and tc 0 from Response Spectra of Large Earthquakes in Greece. Bull. Seism. Soc. Am. 88, 170-182.

Mai P. M. and G. C. Beroza (2003). A hybrid method for calculating near-source, broadband seismograms: application to strong motion prediction. Phys. Earth Planet. Int. 137, 183–199.

Mena B., E. Durukal and M. Erdik (2006). Effectiveness of hybrid Green's function method in the simulation of near field strong motion: an application to the 2004 Parkfield earthquake. Bull. Seism. Soc. Am. 96, S183–S205.

Motazedian D. and G.M. Atkinson (2005). Stochastic finite-fault modelling based on a dynamic corner frequency. Bull. Seism. Soc. Am. 95, 995–1010.

NEHRP, National Earthquake Hazards Reduction Program (1994). FEMA report 222A/223A, Recommended provisions for seismic regulations for new buildings, Provision 1 and Commentary 2, Federal Emergency Management Agency, Washington, D.C.

NTC08, Norme Tecniche per le Costruzioni (2008). DM 140108, Ministero delle Infrastrutture, Roma, Gazzetta Ufficiale.

Olivares L. and F. Silvestri (2001). Analisi della risposta sismica e della subsidenza post-sismica del colle di Bisaccia a seguito del terremoto irpino-lucano del 1980. Proc. X National Conference of ANIDIS. In Italian.

Pacor F., G. Cultrera, A. Mendez and M. Cocco (2005). Finite fault modeling of strong ground motions uing a hybrid deterministic–stochastic approach. Bull. Seism. Soc. Am. 95, 225-240.

Pantosti D. and G. Valensise (1990). Faulting mechanism and complexity of the 23 November 1980, Campania-Lucania earthquake, inferred from surface observations. J. Geophys. Res. 95, 15319-15341.

Pingue F., G. De Natale and P. Briole (1993). Modeling of the 1980 Irpinia earthquake source : constrains from geodetic data. Ann. Geophys. 36, 27-40.

Ripperger J., P.M. Mai and J. P. Ampuero (2008).Variability of near-field ground motion from dynamic earthquake rupture simulations. Bull. Seism. Soc. Am. 92, 2217-2232.

S3 project deliverable D0 (2007). Scenari di scuotimento in aree di interesse prioritario e/o strategico. Deliverable D0: Tecniche di simulazione. http://esse3.mi.ingv.it/deliverables/Deliverables_D0_S3_last.pdf. In Italian.

Siddiqqi J. and G. Atkinson (2002). Ground motion amplification at rock sites across Canada, as determined from the horizontal-to-vertical component ratio. Bull. Seism. Soc. Am. 92, 877–884.

Sørensen M. B., N. Pulido and K. Atakan (2007). Sensitivity of ground-motion simulations to earthquake source parameters: a case study for Istanbul, Turkey. Bull. Seism. Soc. Am. 97, 881-900.

Spudich P. and L. N. Frazer (1984). Use of ray theory to calculate high-frequency radiation from earthquake sources having spatially variable rupture velocity and stress drop. Bull. Seism. Soc. Am. 74, 2061–2082.

Strasser, F. O., N. A. Abrahamson and J. J. Bommer (2009). Sigma: Issues, insights, and challenges. Seism. Res. Lett. 80,41–56.

Toro, G.R., N.A. Abrahamson and J.F. Schneider, (1997) Model of strong ground motions from earthquakes in Central and Eastern North America: best estimates and uncertainties. Seismological Research Letters 68, 1, 41–57

Working Group ITACA (2009). Data base of the Italian strong motion records. http://itaca.mi.ingv.it

Zeng Y., J.G. Anderson and G. Yu (1994). A composite source model for computing realistic synthetic strong ground motions. Geophys. Res. Lett. 21, 725–728.

Zhu T.J., A.C. Heidebrecht, W.K. Tso (1988). Effect of peak ground acceleration to velocity ratio on ductility demand of inelastic systems. Earthq. Eng. Struct. Dyn. 16, 63–79.

Zollo A., A. Bobbio, A. Emolo, A. Herrero and G. De Natale (1997). Modelling of ground acceleration in the near source range: the case of 1976, Friuli earthquake (M= 6.5), northern Italy. J. Seism. 1, 305-319.

Tables

Table 1 – Source and wave propagation processes as modeled in the considered simulation methods.

	Source	Path
1) EXSIM Motazedian and Atkinson, 2005; Boore, 2009	the fault is divided into N sub-faults and each of them is considered as a point source radiating an ω^2 spectrum. Ground motions produced by sub-faults are summed in the time domain, with a proper time delay, depending on the rupture time distribution, to obtain the ground motion from the entire fault. The slip distribution and a constant rupture velocity can be specified.	Stochastic Green's functions: homogenous medium (Vs is specified at the source). Spectral attenuation is defined by geometrical spreading + quality factor + kappa. Frequency-dependent crustal amplification function, to account for waves amplification through the layered model. Distance-dependent duration of seismograms.
2) DSM Pacor et al., 2005; Ameri et al., 2009	An acceleration envelope is computed by the isochrone theory at any give site: the duration is defined by rupture propagation + crustal propagation. The envelope amplitude is modulated for the slip distributions on the fault. The deterministic envelope is then used to window a white noise time series and multiplied by an ω^2 reference spectrum. The finite-fault characteristics as distance, radiation pattern and corner frequency (either apparent or fixed) are parameters of the spectrum.	Semi-stochastic Green's functions: Deterministic envelopes (duration and shape) defined through isochrones for a 1D layered medium. Spectral attenuation is defined by geometrical spreading + quality factor + kappa. Frequency-dependent crustal amplification function, to account for waves amplification through the layered model.
3) HIC Gallovič and Brokešová, 2007	The rupture process at the seismic source is described in terms of slipping of elementary sub-sources with fractal number-size distribution (fractal dimension 2), randomly placed on the fault plane. At low frequencies: based on the representation theorem assuming a final slip distribution composed from the subsources, which is characterized by a k-squared decay. At high frequency, instead, the ground-motion synthesis is obtained summing the contributions from each individual sub-source treated as a point-source. low and high-frequency synthetics are combined in the frequency domain.	Full wavefield Green's functions by DWN technique. Spectral attenuation is defined by quality factor + kappa

Table 2 – Parameters used in the simulation of the Irpinia 0s and of the scenario events. The parameter required and adopted by each method is specified in the relative column (1=EXSIM; 2=DSM; 3=HIC)

	Irpinia earthquake (0s event)	**Methods**
Fault mechanism **	strike: 315° , dip: 60°, rake: -90°	1,2,3
Fault dimensions	length 35 km, width 15 km	1,2,3
fault top depth	2.2 km	1,2,3
Focal depth	10.9 km	1,2,3
Seismic Moment	2 x 10^{19}Nm	1,2,3
Shear wave velocity, Vs	3.2 km/s	1,2
Density, ρ	2.9 gr/cm^3	1,2
Radiation pattern	0.55	1,2
Number of subfaults	along strike:70, along dip:30	1,2,3
Slip distribution **	#1	1,2,3
Nucleation point ** (position from S-E edge)	down-dip:10 km along-strike: 5 km	1,2,3
Rupture velocity (Vr) **	0.8Vs	1,2,3
Stress parameter ($\Delta\sigma$) **	80 bars	1,2
k	0.03 s	1,2,3
Quality factor	100	1,2
Geometrical spreading	1/R	1,2
Distance-dependence duration ***	T_0+0.05R (R>10km)	1
Cross over frequency	0.5-2.0 Hz	3
number of simulations	40	1,2

* In HIC method random variations within +- 30° from the adopted values are prescribed for the high-frequency subsources.
** these parameters are change in the scenario-events simulations, see the main text for details.
*** where T_0 is the subfault source duration defined as $1/f_{0sf}$ (f_{0sf} is the subfault corner frequency)

Table 3.

Ground-motion parameters derived from some accelerometric data recorded during the 1980 Irpinia earthquake. The epicentral distance (R_{epi}) has been evaluated from the 1980 Irpinia earthquake epicenter (41.76N, 15.31E; Working Group ITACA, 2009). The R_{JB} is the distance from the surface projection of the fault as introduced by Joyner and Boore (1981). The R_{JB} distance has been computed with respect to the 0s fault. Only stations with R_{JB} less than 50km are reported. The sites were classified according to the Eurocode 8 (EC8; CEN, 2004) and the Italian Building Code (NTC08, 2008), based on the shear-wave velocity averaged over the top 30 m of the soil profile (Vs30). The EC8 classes are the following: class A, Vs30 > 800 m/s; class B, Vs30=360-800 m/s; class C, Vs30 =180-360 m/s; class D, Vs30 <180 m/s; class E, 5 to 20 m of C- or D-type alluvium underlain by stiffer material with Vs > 800 m/s.

Station	Code	R_{epi} (km)	R_{JB} (km)	PGA_{maxH} (m/s^2)	PGV_{maxH} (m/s)	PGA/PGV (g/ms^{-1})	EC8 class
Bagnoli	BGI	22	7	1.83	0.35	0.54	B
Benevento	BNV	58	28	0.58	0.09	0.64	B
Bisaccia	BSC	28	18	0.95	0.22	0.45	A
Bovino	BVN	54	35	0.47	0.06	0.75	B
Calitri	CLT	19	13	1.72	0.29	0.59	B
Rionero	RNR	36	29	0.97	0.15	0.66	B
Sturno	STR	33	4	3.10	0.70	0.45	B

Table 4

Velocity model used in this simulation study (L. Improta, personal communication, 2007). The model is loosely based on the Amato and Selvaggi (1993) and Improta et al. (2003).

depth (km)	V_P (km/s)	$V_S=v_P/1.81$ (km/s)	density (g/cm^3)	Q_P	Q_S
0	3.5	1.93	2.3	200	100
2	4.5	2.49	2.5	300	150
4	5.7	3.15	2.6	500	200
10	6.5	3.59	2.7	750	250
25	7.5	4.14	2.9	900	300
35	8.1	4.48	3.2	1200	400

Table 5
Regression coefficients for equations (1) and (2) for each of the adopted simulation techniques. Sigma values for the AkB10 model are also reported.

	PGA				PGV			
	DSM_{app}	EXSIM	HIC	AkB10*	DSM_{app}	EXSIM	HIC	AkB10*
a	3.657	3.987	4.121		2.407	2.666	2.831	
c	-1.366	-1.541	-1.592		-0.974	-1.141	-1.314	
σ_K	0.101	0.052	0.095	0.0994	0.091	0.053	0.131	0.1083
σ_A	0.303	0.157	0.129	0.2610	0.272	0.159	0.228	0.2562
σ_{TOT}	0.320	0.165	0.161	0.2790	0.287	0.167	0.263	0.2780

* for AkB10 model the reported values for σ_K and σ_A refer to the inter-event and intra-event standard deviations.

Figure captions

Figure 1

Geometry of the three fault segments whose rupture caused the 1980 Irpinia earthquake. The epicenter of the 0s fault segment is shown by the black star; the fault top is shown by the thick black line. The 10 stations belonging to the Italian strong-motion network within 60 km to the epicenter are represented as triangles (see Table 1 for the station code). Filled triangles highlights the 7 stations that have been used in the strong-motion modeling performed in this study. Black dots indicate the 86 virtual receiver used in the scenario-events simulations. The virtual receivers are within 50 km to the fault surface projection.

Figure 2

K-squared slip distributions and hypocenter locations (white stars) used in the simulations. Slip model in the top panel mimic the one inferred by Cocco and Pacor (1993), characterized by two main asperities, the largest located close to southern edge of the fault and the other to northern edge. This slip is used to model the Irpinia 1980 earthquake ground motions. The largest star represents instrumental hypocenter (40.76°N, 15.31°E). The fault plane is discretized into 70x30 subfaults.

Figure 3

Comparison of North-South(NS) and East-West(EW) recorded and simulated velocity time series at the 7 selected stations (see Figure1) considering the HIC technique. The right panels show the comparison in terms of spectral accelerations (SA) at 5% damping. Time series have been filtered between 0.1 and 12 Hz and the first 20 s of signal has been considered. See Figure S1 for comparison of acceleration waveforms.

Figure 4

Spectral Accelerations, PGV and PGA residuals (black dots), defined as the $\log_{10}$(observed/simulated), considering the geometric mean of NS and EW components are shown for the three simulation techniques. SA residuals are computed for 17 frequencies ranging from 0.25 to 10 Hz. The model bias (black line), defined as the mean of the residuals at each frequency, and relative standard deviation (gray shaded area) are also shown. The bottom-right panel shows a comparison among the model biases computed with the three simulation techniques.

Figure 5

HVSR mean curves (black continuous lines) plus/minus one standard deviation (shaded area) computed for CLT, RNR and STR stations using 6, 3 and 9 records, respectively. The analysis was performed on the S-wave windows selected starting about 1 s before the S-wave onset and ending when 90% of the total energy of the signal has been released, assuming that this interval corresponds to the strong motion phase.

Figure 6

Comparison of simulated and observed spectral accelerations (SA, at 5% damping), geometric mean of NS and EW components, at CLT and STR stations. Left plots: simulations are performed at bedrock. Right plots: site amplification is accounted in the simulations by HVSR-based amplification functions (Figure 5). DSM and EXSIM response spectra are geometrical mean of the 40 realizations.

Figure 7

PGA and PGV values (geometric mean of NS and EW components) for the Irpinia earthquake rupture scenario simulated with HIC (a), EXSIM (b), DSM_{fix} (c) and DSM_{app} (d) techniques. Left columns show the map distribution of peak values and right columns their decay as a function of R_{JB}. The values are simulated at virtual grid points showed in Figure 1. Peak values recorded during the 1980 Irpinia earthquake (classified according to EC8 site classification) are also shown (right columns). The black curves in the right columns represent the median peak values ± 1 sigma predicted by the Akkar and Bommer (2010), AkB10, model for rock sites class and M_w=6.9.

Figure 8

PGA and PGV (geometric mean of NS and EW components) from all earthquake scenarios (black symbols) versus R_{JB} distance. Median PGA and PGV ± σ_{TOT} estimated by equations (1) and (2) are shown by gray curves for DSM_{app}, EXSIM and HIC simulations.

Figure 9

Top: comparison of median PGA and PGV (equation 1) from simulations (DSM_{app}, EXSIM and HIC techniques) and Akkar and Bommer (2010), AkB10, GMPEs for rock site class and M_w=6.9. middle: comparison of PGA and PGV median ± 1 inter-scenario sigma (σ_k) from simulations (HIC method only) and AkB10 median ± 1 inter-event sigma. bottom: comparison of PGA and PGV median ± 1 intra-scenario sigma (σ_A) from simulations (HIC method only) and AkB10 median ± 1 intra-event sigma.

Electronic Supplement description

Figure S1 - Comparison of North-South(left) and East-West(right) recorded (black) and simulated (red) acceleration time series at the 7 selected stations (see Figure1) considering the HIC technique. The right-most panels show the comparison in terms of spectral accelerations (SA) at 5% damping for North-South (continuous lines) and East-West (dashed lines) components. Time series have been filtered between 0.1 and 12 Hz.

Figure S2 – same as Figure S1 but for the DSM technique. Note that, the response spectra are geometrical mean of the 40 realizations.

Figure S3 - same as Figure S1 but for the EXSIM technique. Note that the generic horizontal simulated time series is reported for EXSIM (for the reader's convenience we duplicate the synthetic waveform below recorded NE and EW ones). Consequently the simulated response spectra is for the generic horizontal component. Note that, the response spectra are geometrical mean of the 40 realizations.

Figure S4- Comparison of North-South(left) and East-West(right) recorded (black) and simulated (red) velocity time series at the 7 selected stations (see Figure1) considering the HIC technique. Time series have been filtered between 0.1 and 12 Hz.

Figure S5- same as Figure S4 but for the DSM technique.

Figure S6 - same as Figure S4 but for the EXSIM technique. Note that the generic horizontal simulated time series is reported for EXSIM (for the reader's convenience we duplicate the synthetic waveform below recorded NE and EW ones).

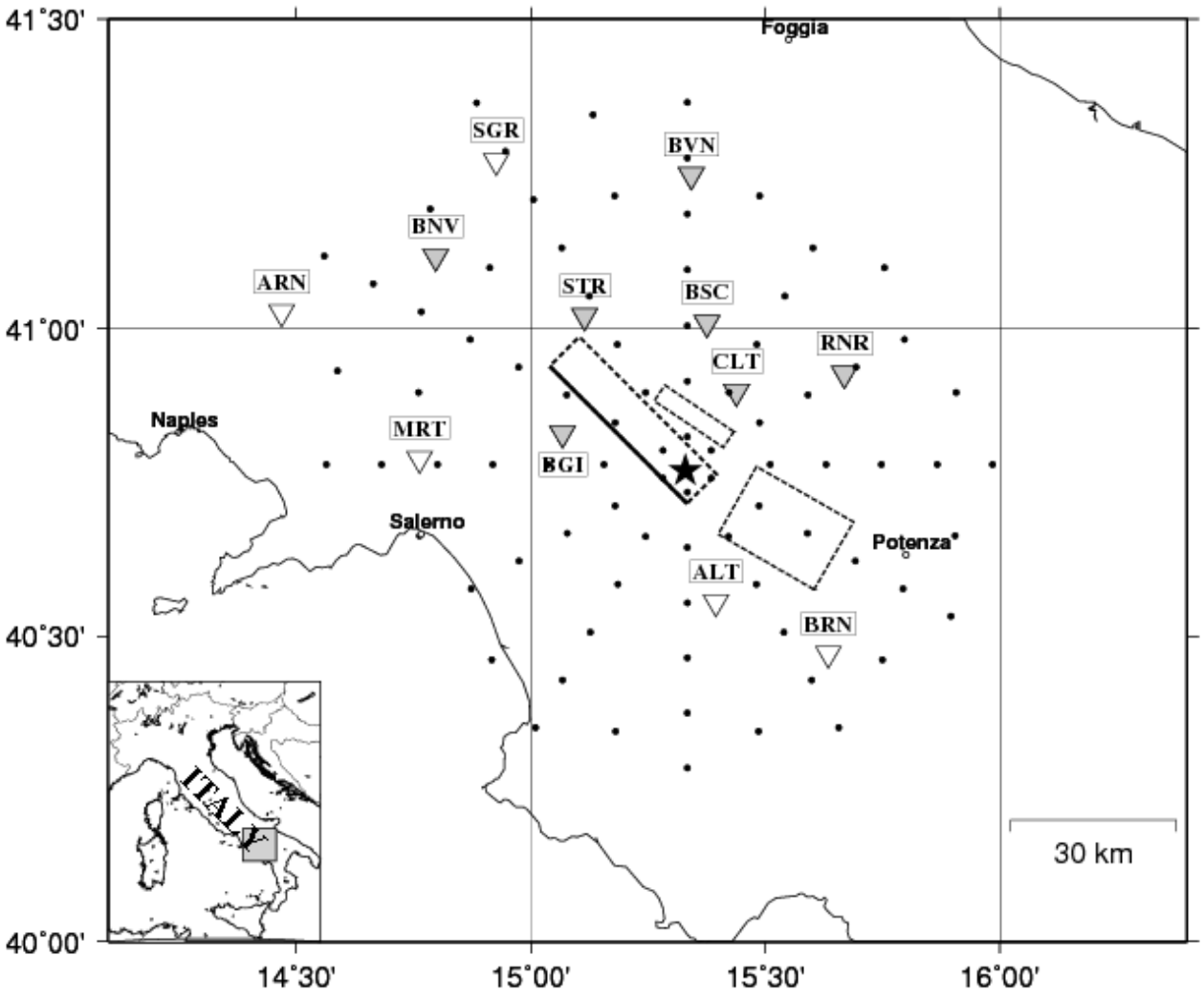
41°30'
41°00'
40°30'
40°00'
14°30'
15°00'
15°30'
16°00'
Foggia
SGR
BVN
BNV
ARN
STR
BSC
RNR
CLT
Naples
MRT
BGI
Salerno
Potenza
ALT
BRN
ITALY
30 km

Figure 1

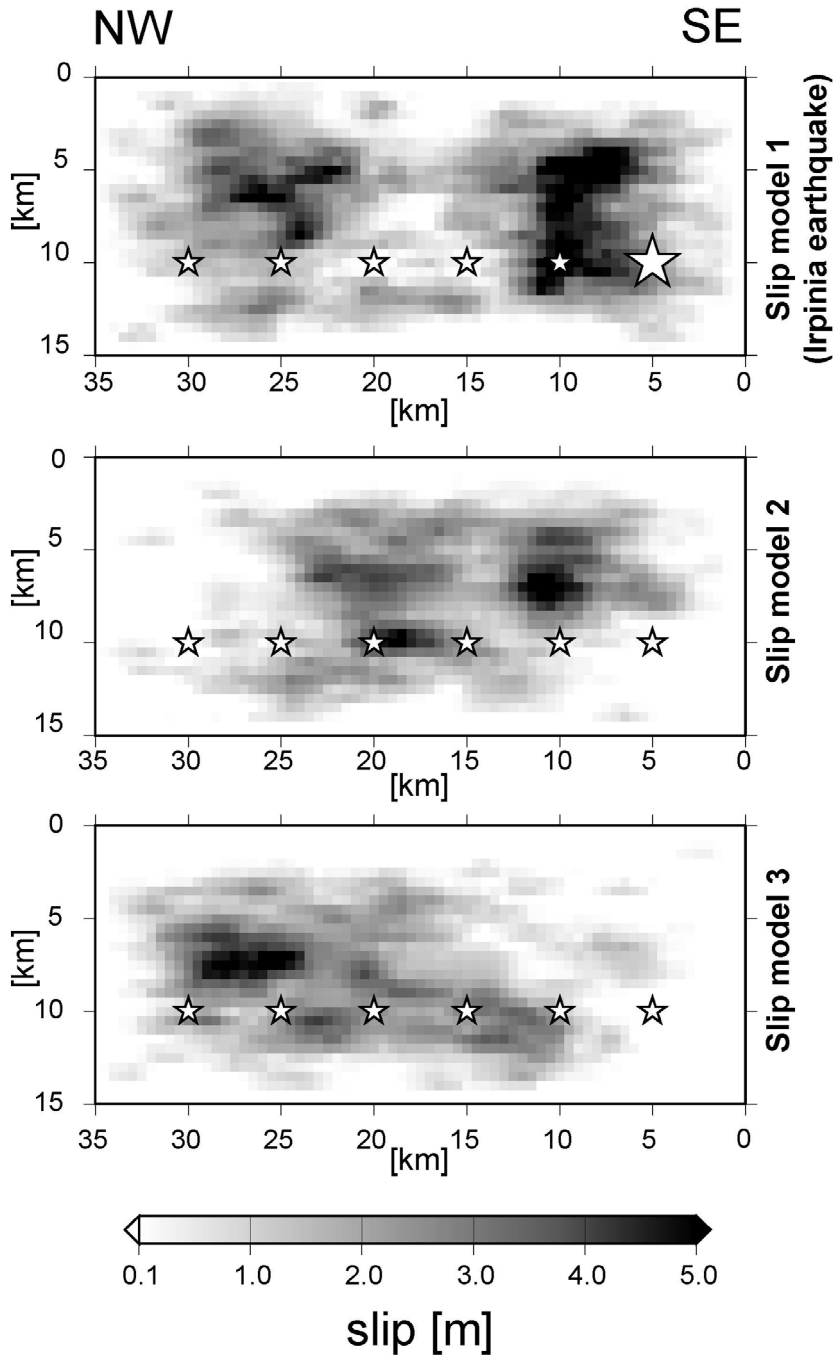
NW
SE
0
5
10
15
[km]
35
30
25
20
15
10
5
0
[km]
Slip model 1
(Irpinia earthquake)
Slip model 2
Slip model 3
0.1
1.0
2.0
3.0
4.0
5.0
slip [m]

Figure 2

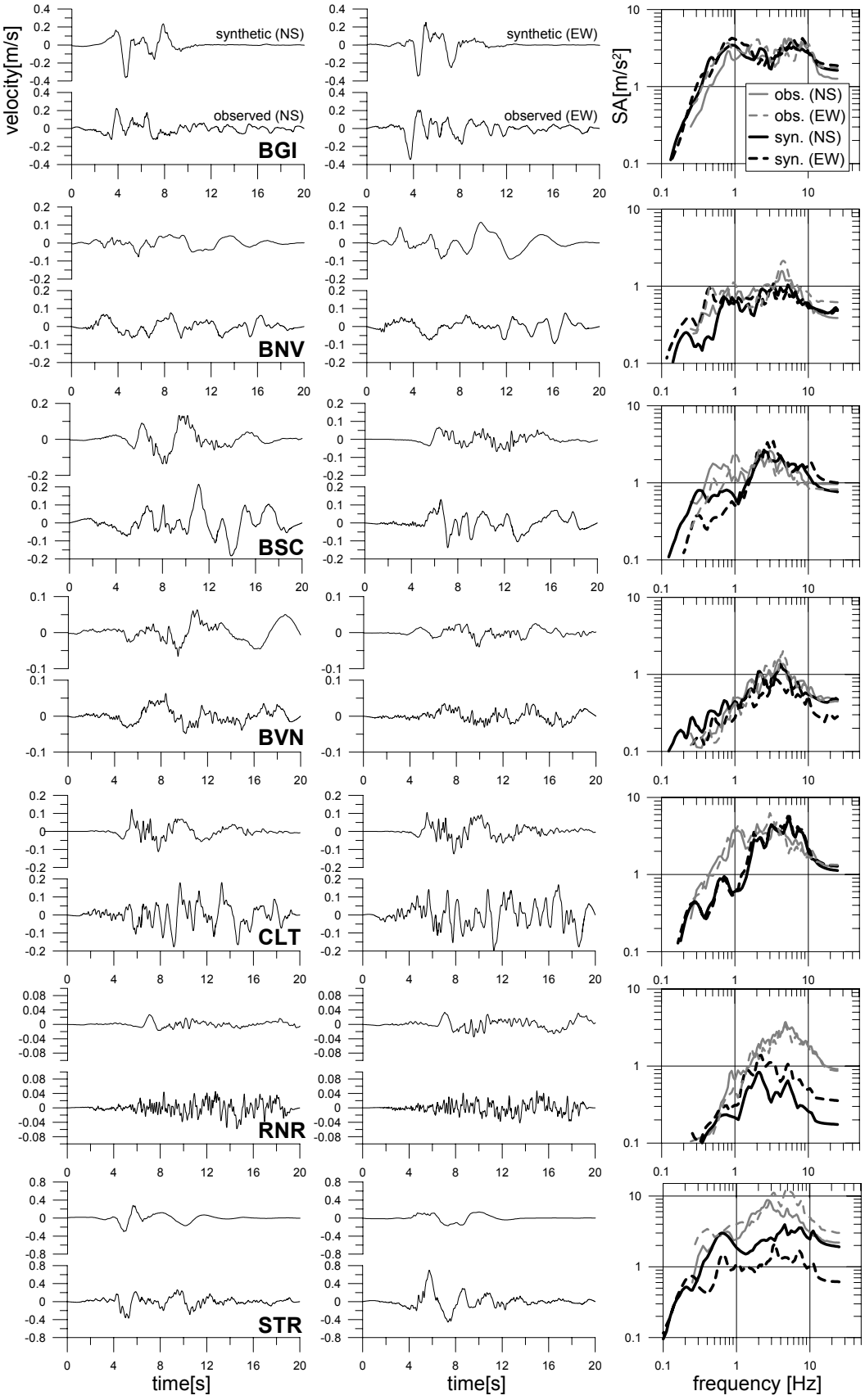
velocity[m/s]
synthetic (NS)
observed (NS)
synthetic (EW)
observed (EW)
BGI
BNV
BSC
BVN
CLT
RNR
STR
SA[m/s²]
obs. (NS)
obs. (EW)
syn. (NS)
syn. (EW)
time[s]
time[s]
frequency [Hz]

Figure 3

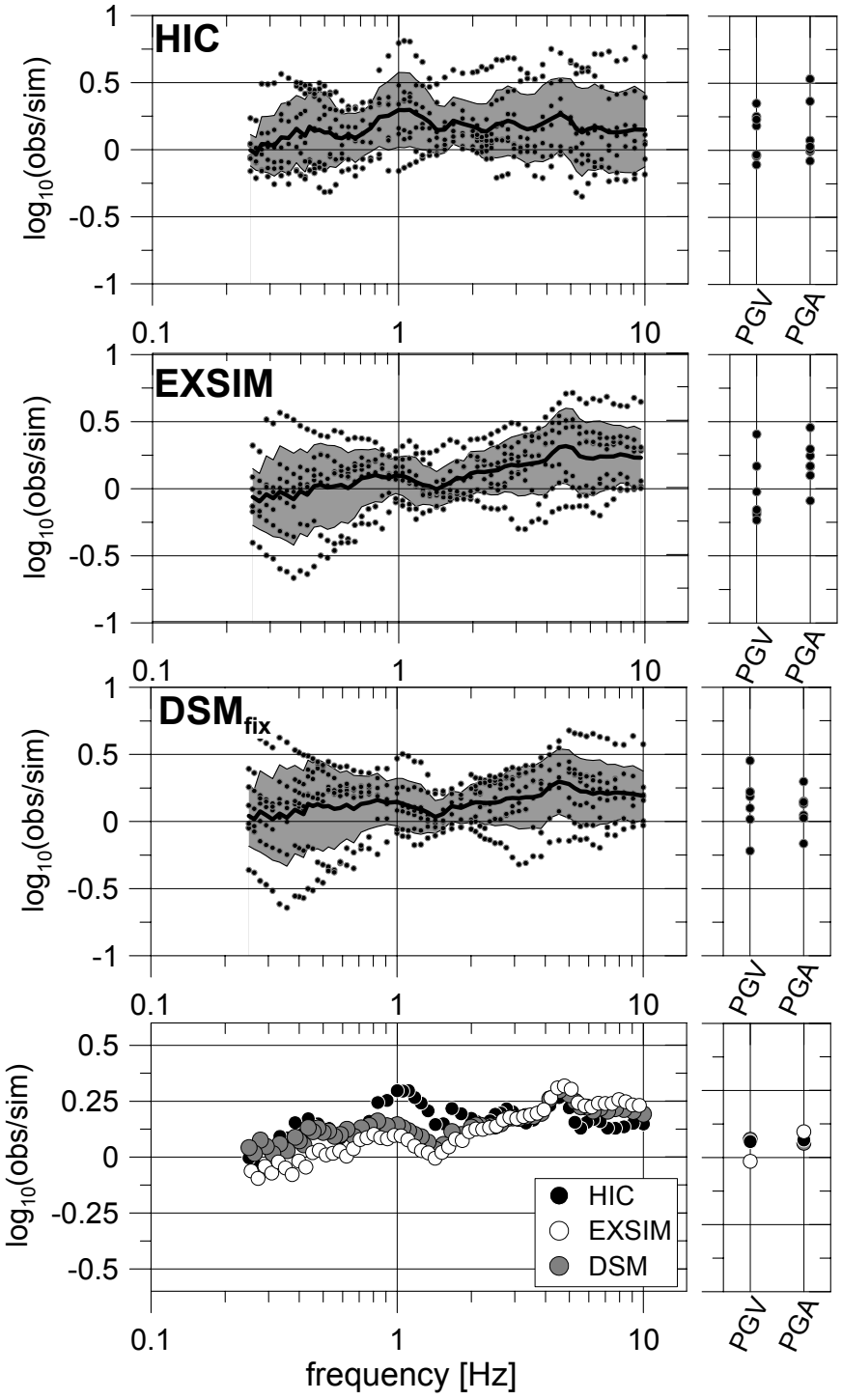
HIC
EXSIM
DSM$_{fix}$
log$_{10}$(obs/sim)
1
0.5
0
-0.5
-1
0.25
-0.25
0.1
1
10
PGV
PGA
HIC
EXSIM
DSM
frequency [Hz]

Figure 4

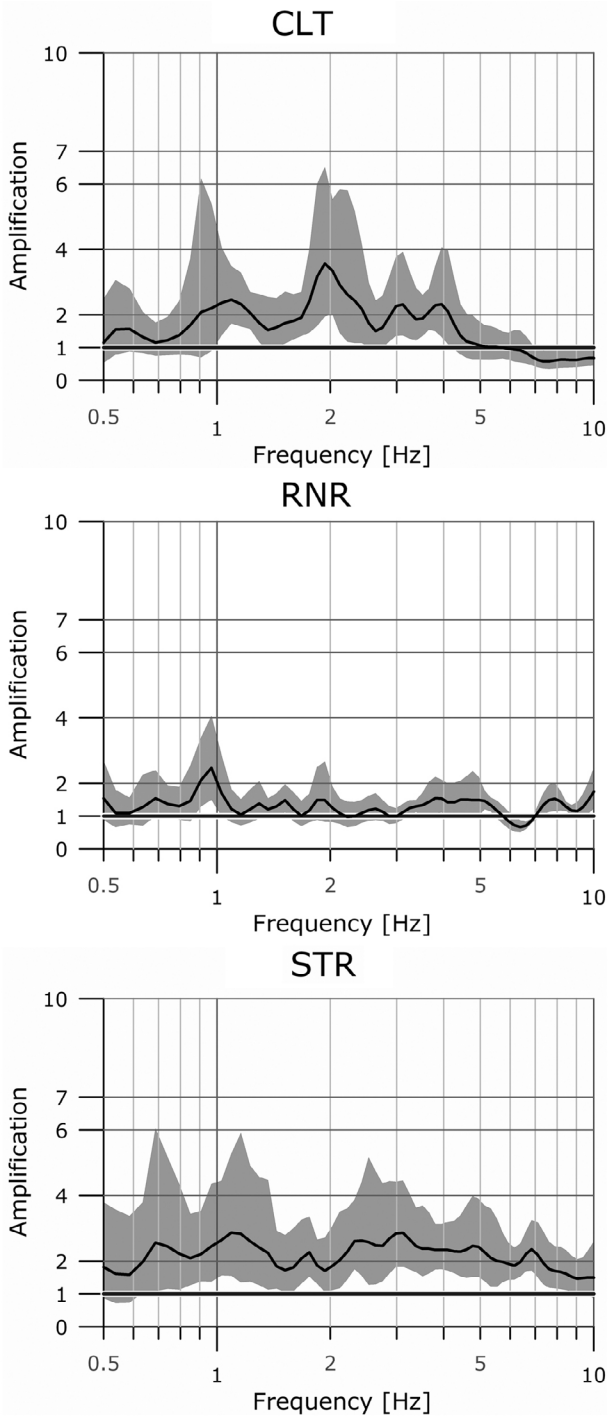
CLT
Amplification
10
7
6
4
2
1
0
0.5
1
2
5
10
Frequency [Hz]
RNR
Amplification
10
7
6
4
2
1
0
0.5
1
2
5
10
Frequency [Hz]
STR
Amplification
10
7
6
4
2
1
0
0.5
1
2
5
10
Frequency [Hz]

Figura 5

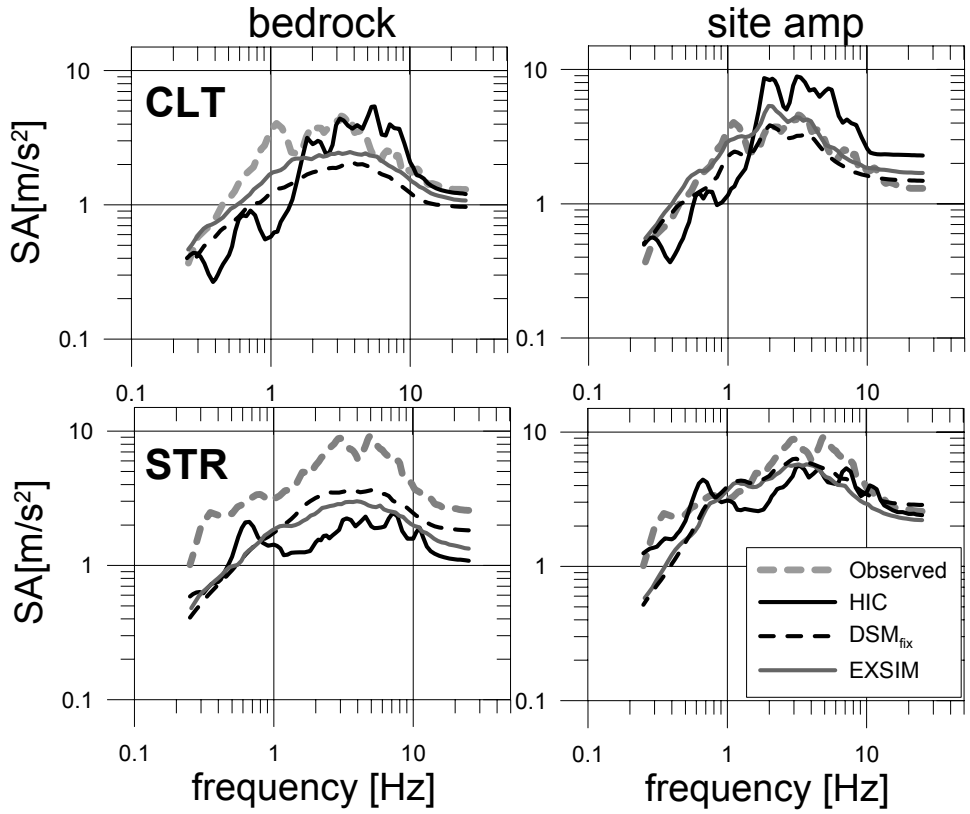
bedrock
site amp
CLT
STR
SA[m/s²]
frequency [Hz]
Observed
HIC
DSMfix
EXSIM

Figure 6

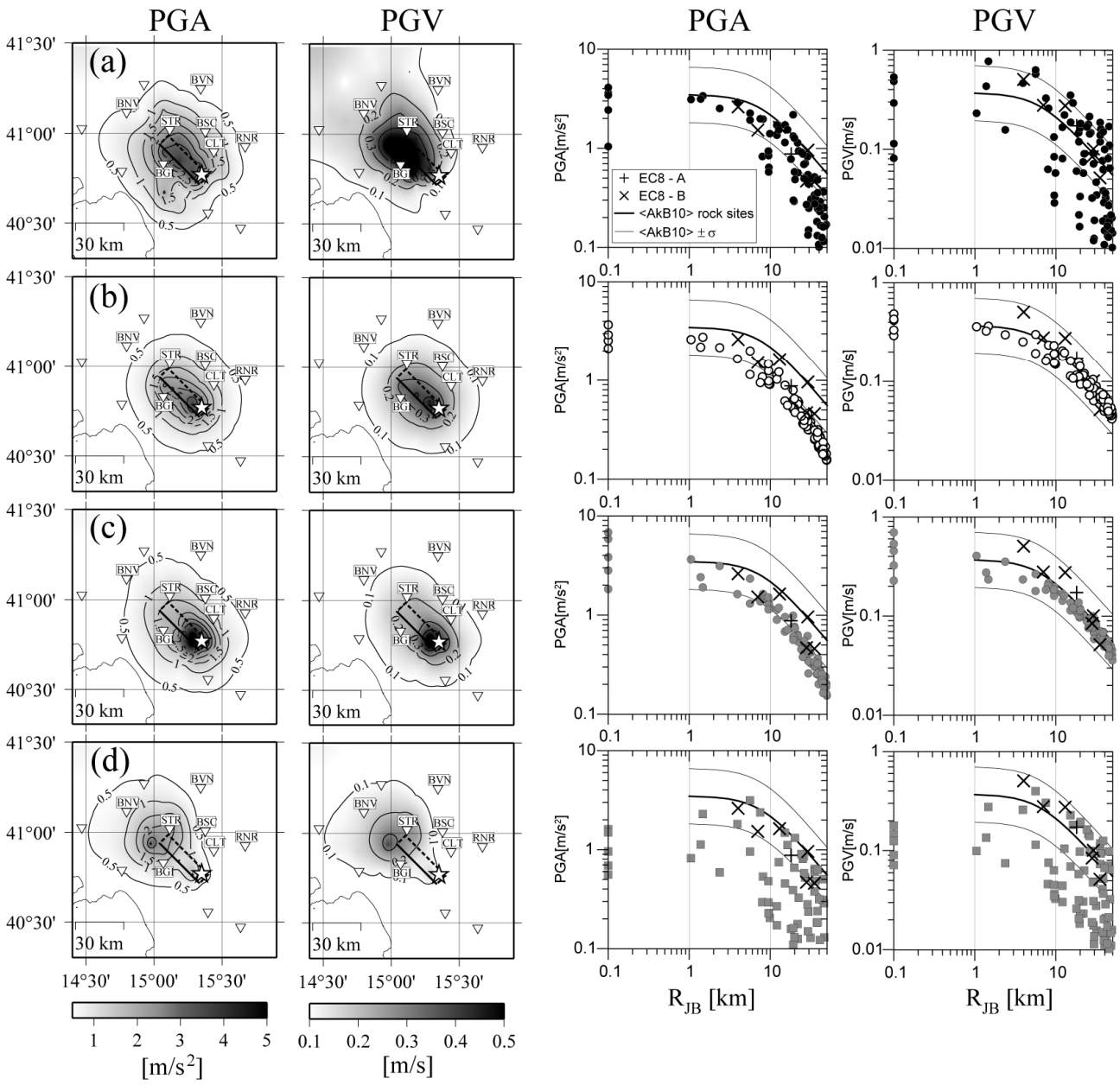
PGA
PGV
PGA
PGV
(a)
(b)
(c)
(d)
BVN
BNV
STR
BSC
CLT
RNR
BGL
30 km
41°30'
41°00'
40°30'
14°30'
15°00'
15°30'
[m/s²]
[m/s]
EC8 - A
EC8 - B
<AkB10> rock sites
<AkB10> ± σ
PGA[m/s²]
PGV[m/s]
R_JB [km]

Figure 7

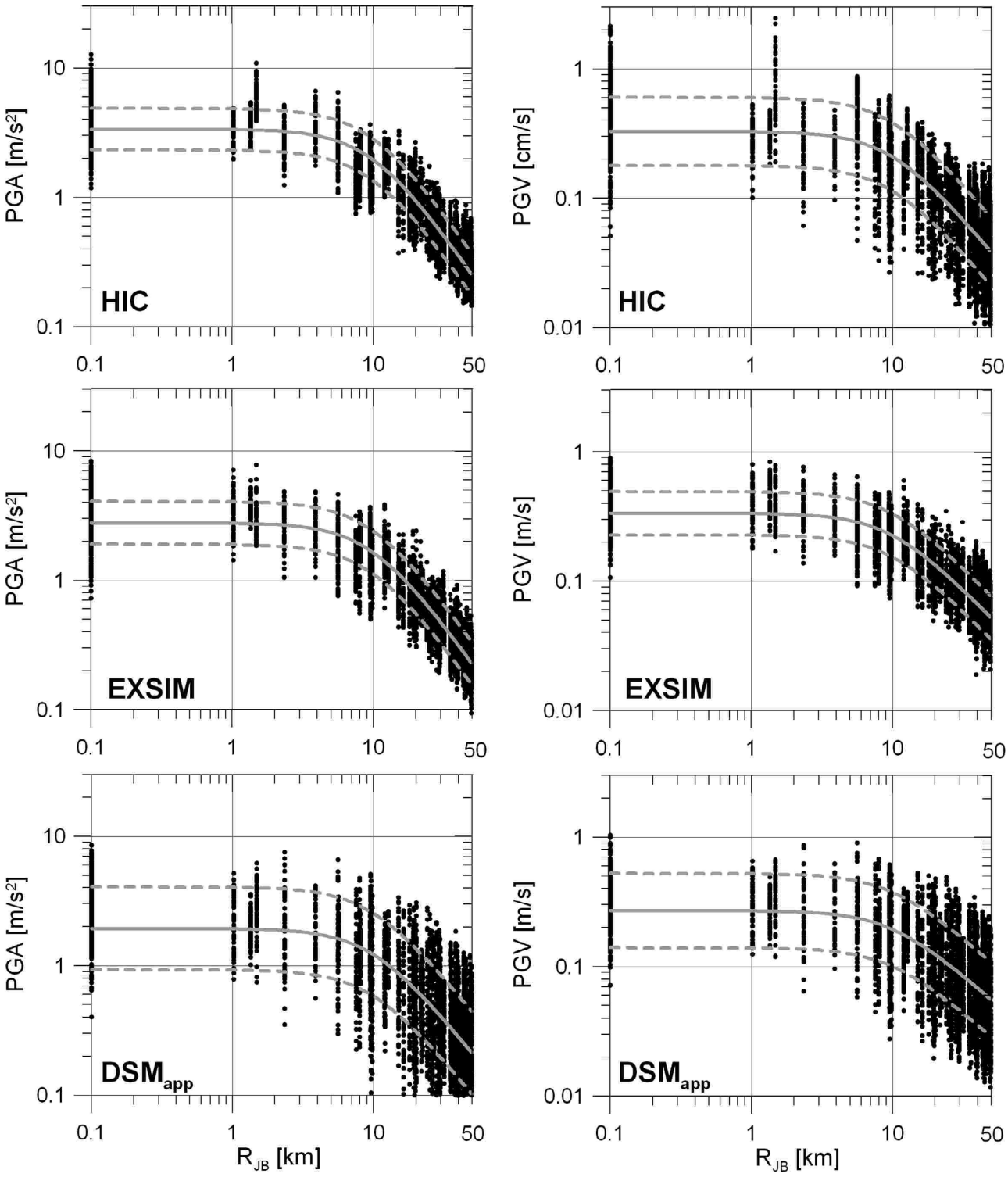

Figure 8

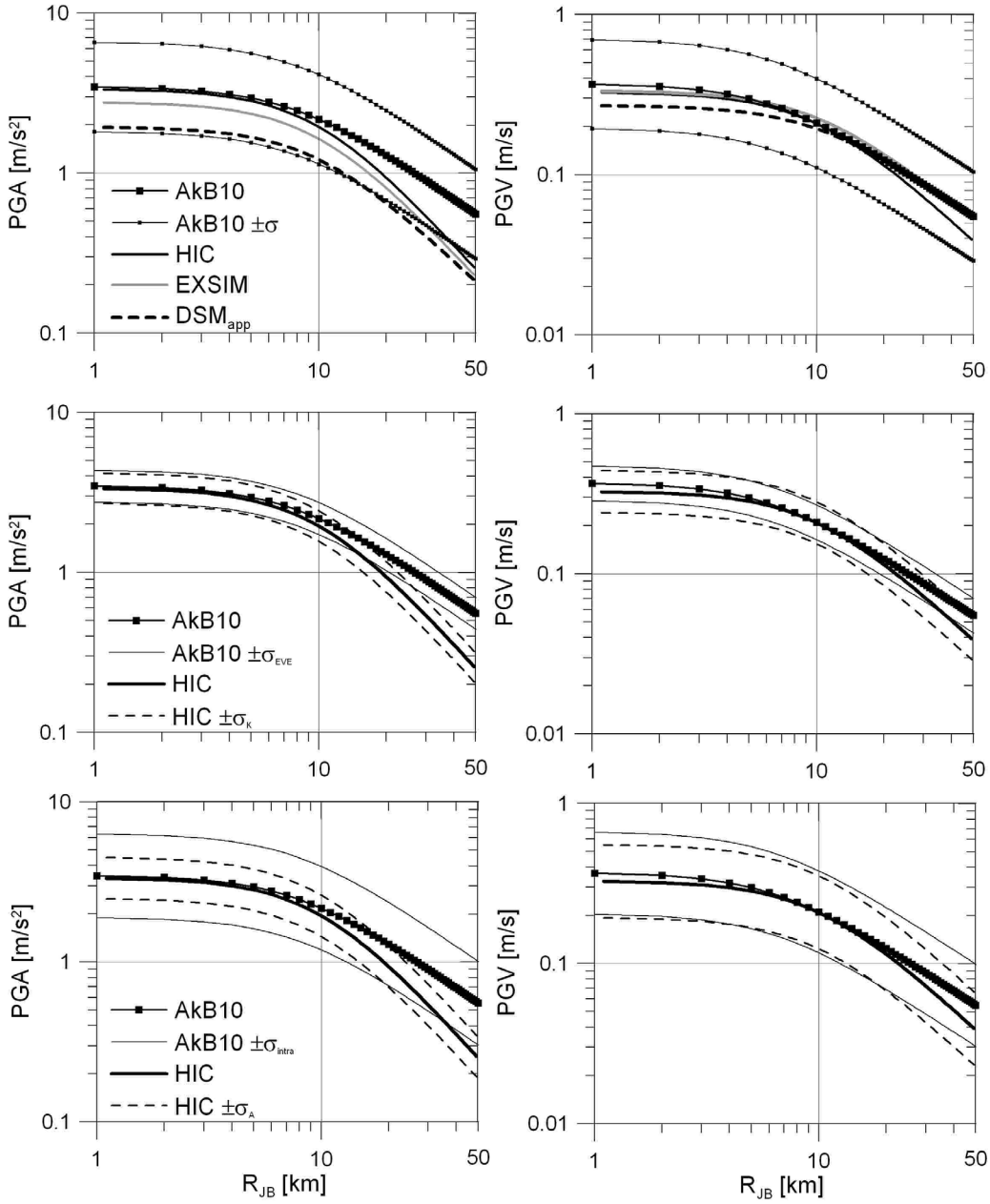
PGA [m/s²]
PGV [m/s]
AkB10
AkB10 ±σ
HIC
EXSIM
DSMapp
AkB10
AkB10 ±σEVE
HIC
HIC ±σK
AkB10
AkB10 ±σintra
HIC
HIC ±σA
RJB [km]
RJB [km]

Figure 9